PROGRESS IN COLOR, COLORANTS AND COATINGS

available online @ www.pccc.icrc.ac.ir

Progress in Color Colorants Coating 18 (2025), 445-459

Ministry of Science, Research and Technology
Institute for Color Science & Technology

Polyaniline-CdSe Quantum Dot Nanostructure: Characterization and Properties

A.M. Arabi[*1], B. Shirkavand Hadavand[2]**

[1.] Department of Inorganic Pigments and Glaze, Institute for Color Science and Technology, P.O. Box: 16765-654, Tehran, Iran

[2.] Department of Resin and Additives, Institute for Color Science and Technology, P.O. Box: 16765-654, Tehran, Iran

ARTICLE INFO

Article history:
Received: 30 Dec 2024
Final Revised: 20 Feb 2025
Accepted: 23 Feb 2025
Available online: 30 July 2025

Keywords:
PANI
CdSe QDs
Nanocomposites
Co-precipitation
Polymerization

ABSTRACT

This research focuses on the synthesis of cadmium selenide quantum dots (CdSe QDs)-polyaniline (PANI) nanocomposites. CdSe QDs were prepared by co-precipitation, and the polymerization process was carried out in the presence of QDs to form an entangled nanocomposite. Structural analysis of the sample revealed the formation of the main PANI peaks along with an amorphous QDs. Chemical analysis confirmed the successful polymerization of PANI and the formation of QD nanoparticles. The thermal behavior of PANI samples with and without QDs showed similar weight loss steps with less weight loss in the presence of PANI, indicating increased thermal stability of the nanocomposite. The microstructure of PANI showed an entangled, coil-like nanorod morphology. Due to this cross-linked structure and the polymerization process, QDs formed as amorphous particles with a uniform distribution within this ordered structure. Structural and microstructural studies emphasized the presence of NaCl impurity. The optical behavior of CdSe QDs synthesized at different temperatures from 70 to 100 °C showed that increasing the temperature shifts the emission to lower energy regions. The emission spectrum of the composite sample showed that the blue emission peak at around 420 nm is due to the π-π electronic transition in polyaniline. With increasing the QD concentration to 10 % by weight relative to polyaniline, the formation of green emission spectrum of QDs due to the electronic transition between these two luminescent centers reduced its intensity. These results indicate that due to the proper entanglement, the obtained product can be a suitable candidate for electroluminescent applications. Prog. Color Colorants Coat. 18 (2025), 445-459© Institute for Color Science and Technology.*

1. Introduction

Quantum dots (QDs) have increasingly found applications in advanced technologies, including light-emitting diodes, sensors, lasers, detectors, and bio-imaging [1-5]. Future prospects include novel lasers, medical imaging, and quantum advancements [1]. Among various types of QDs, their nanocomposites are currently undergoing significant development for various applications [3]. The simultaneous use of organic-inorganic compounds can lead to the production of QDs with much better dispersion, uniformity, and controllability [4]. Surface modification of QDs using covalent and non-covalent bonds significantly influences various properties, including drug delivery [5]. Furthermore, surface modification of QDs for dispersion in polymer matrix is another commonly employed

*Corresponding author: * aarabi@icrc.ac.ir; ** shirkavand@icrc.ac.ir

https://doi.org/10.30509/pccc.2025.167441.1348

nanocomposite approach, leading to improved properties of epoxy polymer films [6].

Polyaniline (PANI) is a conjugated polymer renowned for its good electrical conductivity, environmental stability, flexibility, and cost-effectiveness [7, 8]. The electrical conductivity in PANI is attributed to both electron and hole carriers, exhibiting non-ohmic behavior [9]. One of the most extensively researched QDs-based materials is the polyaniline-quantum dot (QDs-PANI) nanocomposites. Various oxide and non-oxide compounds have been utilized for compositing with PANI including oxide QDs of cobalt, silver, and zinc [10], carbon quantum dots (CQDs) [11], gold nanowires-graphene quantum dots (GQDs) [12], silver nanoparticles, and graphene oxide quantum dots (GOQDs) [13], and functionalized GQDs [14].

A variety of innovative techniques has been employed for synthesizing quantum dot-based nano-composites. These methods include sol-gel [10], electrodeposition [11], hydrothermal pyrolysis and interfacial polymerization [12], in-situ oxidative chemical polymerization of aniline in the presence of nanoparticles and QDs [13], oxidative polymerization of aniline in the presence of PbS [14], and in-situ emulsion polymerization [15].

PANI-QDs nanocomposites exhibit a multi-functional nature and have been reported to have a wide range of applications due to their absorption, magnetic, electrical, thermal, photoluminescent, antibacterial, and anti-corrosion properties [10]. PANI-QDs, in the form of dual or multiple nanocomposite structures, have been utilized in dye-sensitized solar cells (DSSCs), supercapacitors, gas sensors, biosensors, and imaging. Energy storage using supercapacitors has been a subject of significant interest among researchers [11]. Identifying cancer at its initial stages using immunosensors [11], optical sensors [13], hydrogen production [14], and improved photo-electrochemical behavior and corrosion protection using cathodic protection coatings [16] are among other reported applications.

One of the most important groups of QDs is CdSe, and the construction of such composites with PANI has been of interest. It has been stated that PANI-CdSe QDs complexes can be widely used in solar cells, aerospace, microelectronics, automotive, communi-cations, biomedicine, and textiles [17]. In solar cells, the use of PANI as a filler layer for pinholes in CdS/CdTe solar cells improves open-circuit voltage and fill factor [18]. Also, PANI, as an electron donor in CdSe acceptor solar cells, improves energy efficiency [15]. Ternary nanocomposites have also shown unique properties in this regard, as an example in photophysical properties. Laponite/CdSe/polyaniline has the ability to achieve broad-spectrum visible emission, which is useful for LEDs and solar cells [8]. Another ternary composite, Nafion/CdSe/self-doped polyaniline (SPAN), exhibits electrocatalytic behavior and has the ability to detect dopamine (DA), uric acid (UA), and ascorbic acid (AA) [19]. Due to the charge transfer between PANI and CdSe QDs, the relaxation process leads to the termination of radiative recombination and consequently the quenching of emission [17].

Advanced techniques have been used for the synthesis of CdSe QDs-PANI nanocomposites. The synthesis of quantum dots in this method is carried out in the presence of trioctylphosphine oxide (TOPO) at 280°C by reacting cadmium stearate and powdered selenium dissolved in trioctylphosphine (TOP), followed by separation, purification, and redispersion in hexane and chloroform, and then mixing with PANI in hexane [17]. However, due to the high complexity, the need for controlled conditions and expensive raw materials, and the difficulty of controlling the process at high temperatures, these nanocomposites have lower commercialization potential.

Hydrothermal methods seem to be more favorable due to the low cost of raw materials, the ability to control temperature and pressure, the management of the compositing stage through surface modification and creation of electrostatic tendencies, as well as the use of industrial equipment for the synthesis. Researchers have focused on important factors such as reducing agents (sodium borohydride, ascorbic acid, tri-sodium citrate dehydrated, tartaric acid, and 2-amino-benzenecarboxylic acid), the concentration of the surface modifier (3-mercaptopropionic acid), pH value, and the concentration of raw materials in the hydrothermal synthesis of QDs [20, 21]. However, there are limited research on the optimal conditions for low-temperature precipitation method (below 100°C), especially in the presence of compounds such as PANI.

In this research, low temperature co-precipitation method (below 100°C) and the subsequent poly-merization were applied for the formation of CdSe QDs and their nanocomposites with PANI. The chemical, thermal, structural, morphological, and

optical properties of these nanocomposites and their constituents were also evaluated.

2. Experimental

2.1. Materials

All chemicals used, including cadmium chloride ($CdCl_2$), selenium dioxide (SeO_2), sodium boro-hydride ($NaBH_4$), mercaptopropionic acid (MPA, $HSCH_2CH_2CO_2H$), aniline ($C_6H_5NH_2$), ammonium persulfate ($(NH_4)_2S_2O_8$), and hydrochloric acid (HCl), were of analytical grade.

2.2. Synthesis of hybrid materials

2.2.1. Synthesis of CdSe QDs

Quantum dots were synthesized using the co-precipitation method. In the first step, 0.056 g of selenium oxide and 0.2 g of cadmium chloride were dissolved in 50 mL of deionized water. After a period of stirring, 0.02 g of $NaBH_4$ was added to the solution. At this stage, 0.009 g of MPA was added, and after 30 min of degassing, the synthesis steps were continued for 2 hours under a nitrogen atmosphere using a reflux system and applying heat in the range of 70 to 100°C. To examine the powder form of the quantum dots, they were precipitated by using a solvent such as acetone.

2.2.2. Synthesis of CdSe QDs-PANI nano-composites

5% by weight of CdSe QDs was dispersed in 20 mL of deionized water relative to the PANI. A solution containing the QD nanoparticles, 2 mL of aniline, and 50 mL of 1 M HCl was added to a 250 mL flask. The temperature was maintained at approximately 0°C using an ice bath. 5 g of ammonium persulfate was dissolved in 50 mL of 1 M HCl solution and added dropwise to the aniline solution. The solution was kept at 0°C for 5 h to ensure the completion of the reaction. Then, the product was filtered and dried at 60°C for 24 h for the subsequent characterization. A sample containing 10% by weight of QDs was also prepared for comparing the luminescent properties. For the preparation of these composites, only the CdSe QDs with the highest emission intensity synthesized at 90 °C were used.

2.3. Materials characterization

To investigate the chemical composition, Fourier Transform Infrared Spectroscopy (FTIR, Perkin Elmer Spectrum One) was used. To determine the glass transition and decomposition temperatures, differential scanning calorimetry (DSC, PerkinElmer Pyris 6) was employed. For thermal analysis, simultaneous thermal analysis (STA, PerkinElmer Pyris Diamond) was utilized. The morphology of the products was examined using a scanning electron microscope (ZEISS and Tescan instruments). For a more detailed investigation of the quantum dot nature of the particles, transmission electron microscope (TEM, Zeiss EM900) was used. The optical behavior of the quantum dots was studied using a PerkinElmer Lambda 25 UV-Visible spectrophotometer and an LS55 luminescence spectrometer. The band gap was obtained using the Tauc method by plotting the $(\alpha h\nu)^{0.5}$ curve versus hν, where α is the absorption coefficient and hν is the photon energy in eV. Then, the band gap can be determined by extending the linear part of the curve and extrapolating it to intersect the hν axis.

3. Results and Discussions

3.1. Structural studies

Figure 1 shows the X-ray diffraction pattern of the quantum dot sample. The observed amorphous background is related to the formation of quantum dots. Because their size is below the Bohr radius, CdSe QDs do not exhibit a distinct crystalline phase in diffraction patterns. The observed peaks correspond to NaCl consistence with standard card 0628-005. The formation of this phase is related to the sedimentation stage of the QDs. Due to the presence of sodium and chloride from $NaBH_4$ and $CdCl_2$, respectively, the formation of this structure is quite plausible. This impurity is removed during the subsequent purification and washing steps.

Figure 2 shows the X-ray diffraction pattern of the QDs-PANI nanocomposite. After compositing, the amorphous state is more evident with a broader peak, which is related to the polymerization method. The peaks at 21˚ and 25˚ correspond to PANI and are attributed to polymer interactions and momentum transfer in a specific direction (perpendicular to the polymer main chain) [22]. Chemical analysis of polyaniline reveals the presence of benzenoid and quinoid groups within PANI chain.

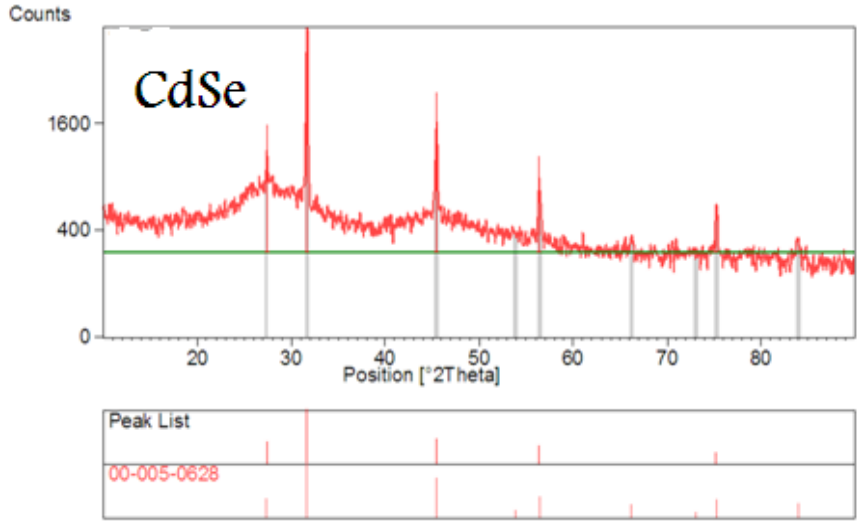

Figure 1: XRD pattern of CdSe QDs.

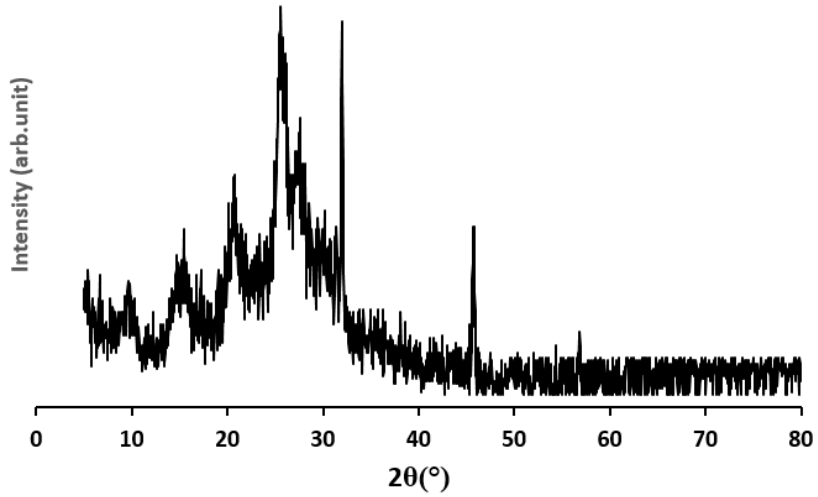

Figure 2: XRD pattern of CdSe QDs-PANI nanocomposite.

The alternating repetition of these two rings induces a semi-crystalline state in the conducting polymer. In polyaniline, this results in crystallization peaks in the range of 10-30°. This crystallinity is observed in both directions parallel and perpendicular to the polymer's main chain. The combination of high electrical conductivity in quinoid groups and low electrical conductivity in benzenoid groups creates selective conditions for momentum transfer along two perpendicular directions within the polymer chain [23]. The filtered product was analyzed immediately. The persistence of NaCl peaks at 27°, 32°, 45°, and 57° suggests that the CdSe QDs-PANI nanocomposite is sensitive to multiple washing steps required for salt removal. The formation of PANI occurs homogeneously without phase separation. The absence of any other peak suggests that the QDs do not interfere with the polymerization of PANI or cause any structural disruptions.

3.2. Chemical composition

As shown in Figure 3, the FTIR spectrum of the quantum dot is mainly composed of peaks related to MPA. The presence of a peak around 720 cm^{-1} confirms the formation of CdSe bonds [24]. However, the intense peaks at 1580 and 3400 cm^{-1} are attributed to water bonds. A peak at 1730 cm^{-1} can be assigned to carboxyl groups of MPA. The lack of a peak at 500 cm^{-1} (S-S bond of MPA) suggests that the carboxyl groups have coordinated with the quantum dot surface instead of the attachment of MPA to the Cd ions on the surface of QDs. The absence of the peak of thiol

groups at 2550 cm^{-1} in the spectrum suggests a surface reaction of MPA with QDs [25].

The FTIR spectrum in Figure 4 indicates the characteristic peaks of PANI structure. The important absorption peaks are located at 3444, 2963, 1631, 1456, 1261, 1096, and 804 cm^{-1}. The peak at 3444 cm^{-1} is characteristic of N–H in the composition and the peaks at 2963 and 2927 cm^{-1} are related to aromatic C–H bond. The peaks at 1631 and 1456 cm^{-1} correspond to the C=C bond in quinoid and benzenoid rings, respectively. Additionally, the peaks at 1261 and 1096 cm^{-1} indicate C–N in benzenoid. The peak at 804 cm^{-1} indicates the C–H bond. Other weak peaks such as 1145-1161 cm^{-1} are related to the bending vibration of C-H bond. Additionally, weak peaks at 1050 and 690 cm^{-1} are related to the stretching vibrations of sulfonate groups (S=O and S–O) [26].

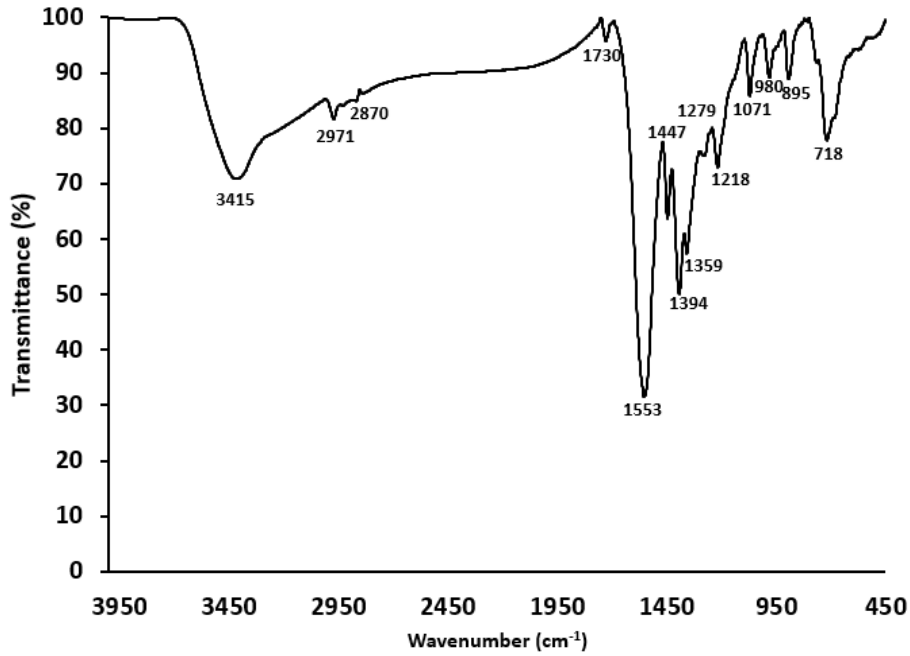

Figure 3: FTIR spectrum of the CdSe QDs.

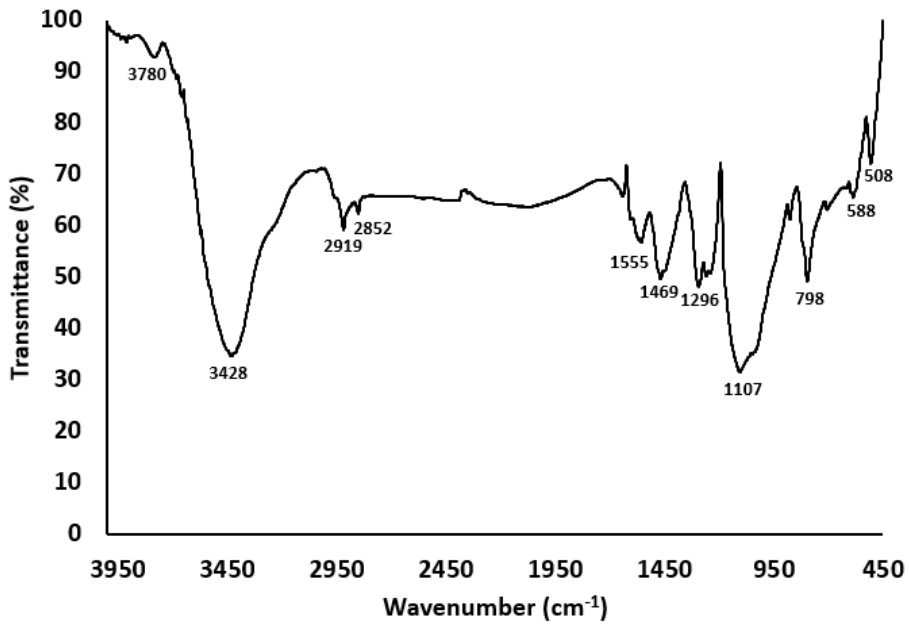

Figure 4: FTIR spectrum of the PANI.

3.3. Thermal analyses

3.3.1. Simultaneous Thermal Analysis (STA)

Figures 5 and 6 present the STA graphs of PANI and CdSe QDs-PANI nanocomposite, respectively. Both samples were analyzed under nitrogen atmosphere. When comparing the two samples, similar weight loss steps are observed. The main weight losses occur in three steps in accordance with the TG, DTA, and DTG curves. The first step, below 100°C, is related to the loss of water, which is an endothermic peak. In the second step, in the range of 150-300°C, impurities, chemically bound water, and unreacted monomers are decomposed. Due to a degradation of different compounds, the DTG curve in the second step consists of two peaks. A peak around 200°C corresponds to the loss of chemically bound water, and a peak around 270°C corresponds to monomers and other organic impurities [22]. The weight loss in the third step, which is the most important stage and has a steeper slope, is due to the decomposition and degradation of the PANI backbone and loss of HCl as a dopant of PANI [27]. A slow and gradual weight loss is also observed between the second and third stages. It seems that from the beginning of the removal of organic impurities or non-alkyl groups, such as methoxy and ethoxy, the thermal decomposition process continues steadily. According to the broad DTA curve, endothermic behavior is observed before 200°C [28, 29]. From this stage onwards (200-600°C), there are two broad exothermic peaks. This indicates that the exothermic peak related to the removal of other factors and groups is completely distinct from the PANI backbone. In the CdSe QDs-PANI nanocomposite, higher thermal stability is observed, and the final weight loss at 600°C for PANI and CdSe QDs-PANI nanocomposite is 51.46% and 61.56%, respectively. In other words, the overall shape of the curves shows a similar trend in thermal behavior. However, the composite sample exhibits higher thermal stability [22]. This can be attributed to the physical and chemical interactions between PANI and QDs.

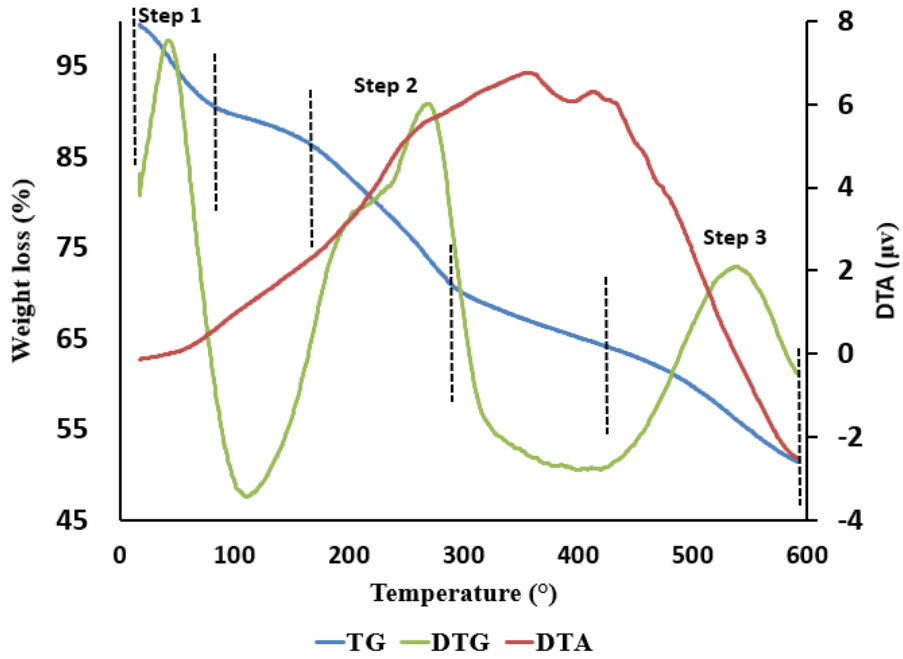

Figure 5: STA graphs of PANI.

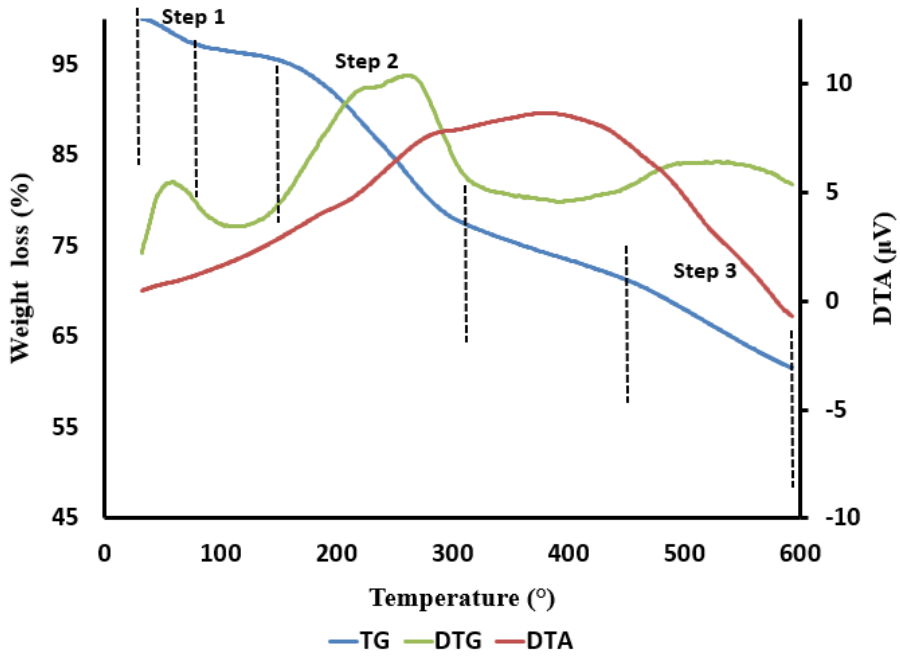

Figure 6: STA graphs of CdSe QDs-PANI nanocomposite.

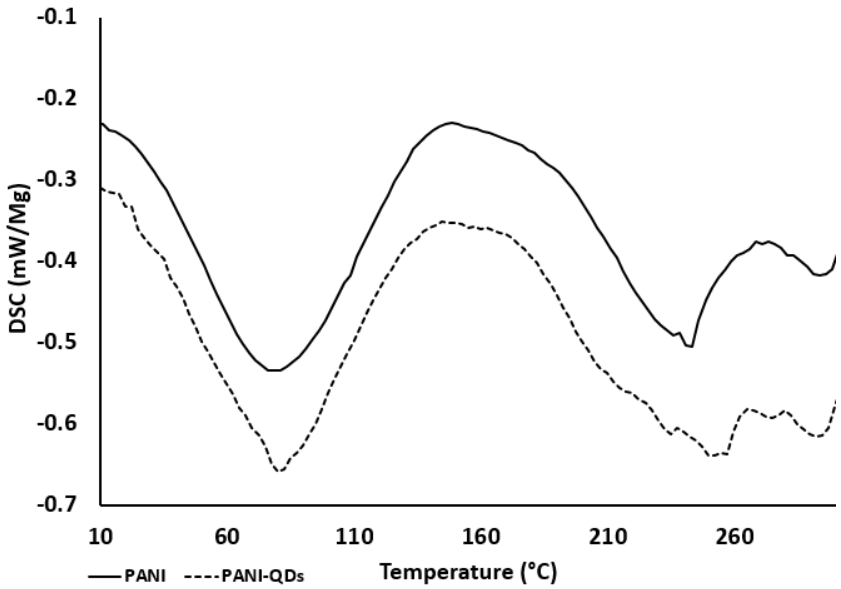

Figure 7: DSC analysis of PANI and CdSe QDs-PANI nanocomposite.

3.3.2. Differential scanning calorimetry (DSC) analysis

Thermal analysis was done in a nitrogen atmosphere at a heating rate of 10°C per minute, from 0°C to 300°C. The DSC curves of PANI and CdSe QDs-PANI nanocomposite are shown in Figure 7. The T_g in both samples was estimated to be in the range of 31-33°C. HCl-doped PANI has been shown to exhibit a T_g of 36°C. The reason for the difference is due to the amount of HCl and water, and consequently, the molecular weight (MW) of PANI in different synthesis methods. Comparing the PANI and CdSe QDs-PANI nanocomposite, many similarities and identical steps are seen. In both samples, two endothermic peaks are observed at 80 and 240°C, with the first peak related to

the loss of volatile substances and physical water, and the second peak due to bound water, organic impurities, and monomers. Most of the differences occur in temperature ranges above 200°C [27]. In this range, the endothermic peak intensities are reduced; particularly above 250°C, the weak multiple-peak behavior in CdSe QDs-PANI nanocomposite replaces the strong single peak of PANI. This confirms the increased thermal stability in the presence of CdSe QDs.

3.4. Morphological studies

SEM images of the PANI sample are presented in Figure 8. The nanofiber morphology in the micro-structure is clearly observed. These fibers have an entangled honeycomb-like structure and are composed of finer fibers on the nanometer scale [30]. The agglomeration of fine fibers creates cavities, which is a very suitable shape for creating nano-hybrids with quantum dots. PANI is prepared in an acidic environment, and strong interactions between the charged chains lead to the formation of nanorods [31]. Figures 8b and 8c show the FESEM image of PANI nanorods at higher magnifications, precisely illustrating the aggregation, entanglement, and cross-linking of these nanorods as well as the formation of cavities. The majority of the nanorods have a diameter below 20 nm. The morphology also indicates that the temperature and reaction time conditions of the polymerization are suitable for the formation of nanofibers. This form of particles can be appropriate for hosting QDs. Increasing temperature and time leads to an increase in the diameter of the nanorods and the creation of sheet-like and flower-like nanoparticles [32], which are not suitable as a composite matrix.

SEM images of CdSe QDs-PANI nanocomposite are presented in Figure 9. Agglomerates of CdSe QDs nanoparticles are clearly observed among PANI nanofibers. The fibers exhibit a highly cross-linked state, while the QDs have amorphous and spherical shape. In the backscattered electron images, due to the difference in molecular weight between CdSe and PANI, the QDs appear as brighter particles. The small size of the quantum dot particles is due to the use of capping agents and surfactants, which leads to their suspension in the aqueous media. In order to form the composite, it is necessary to precipitate the suspended particles by using precipitating agents. At this stage, the quantum dots strongly agglomerate due to their hydrophilic nature and the presence of strong capillary attractions (due to the high specific surface area). In addition, these particles have a semi-crystalline state (see XRD pattern in Figure 1). The final state and form of these amorphous irregular agglomerates are preserved during the polymerization process due to the use of water media. However, the distribution of these particles in the PANI matrix appears to be regular, which is due to the honeycomb-like morphology of PANI.

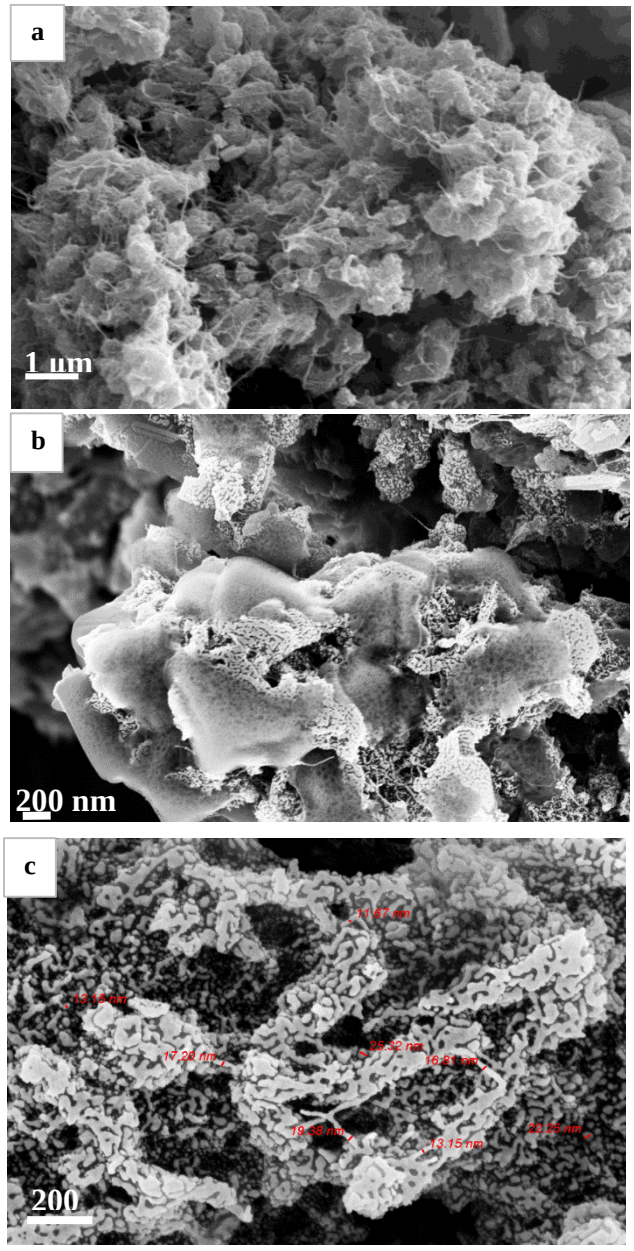

Figure 8: (a) SEM, and (b,c) FE-SEM images of PANI at different magnifications.

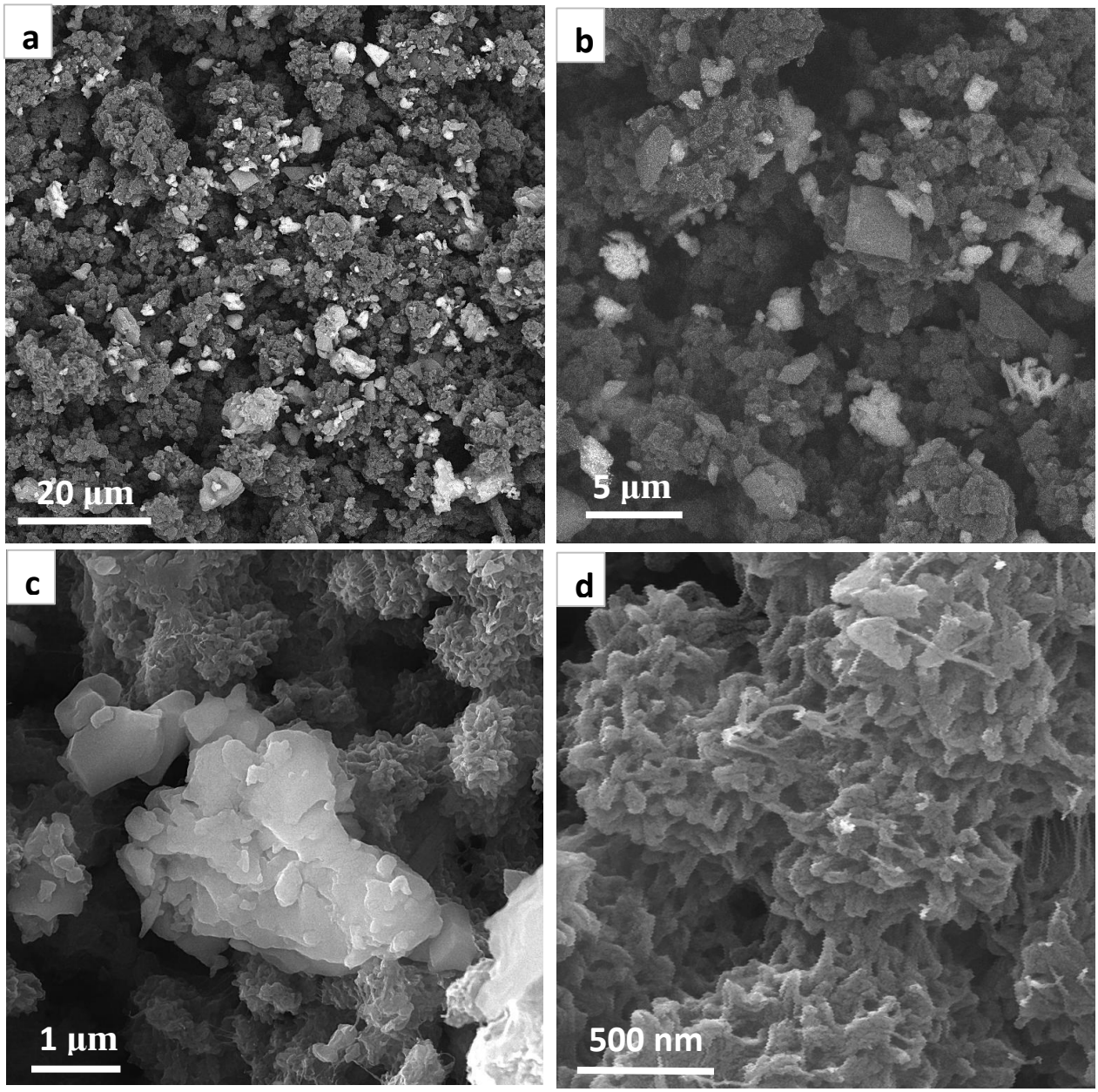

Figure 9: FESEM images of CdSe QDs-PANI nanocomposite at different magnifications: (a, b) backscattered and (c, d) secondary electron images.

EDX and elemental mapping analyses (Figures 10 and 11, respectively) were used to further examine the distribution and entanglement of nanoparticles within the nanocomposite. The results obtained from a region with a brighter mass compared to the PANI background show that the particles are composed solely of Cd and Se, with the presence of S attributed to a CdS capping layer formed from the reaction of $CdCl_2$ and MPA. Na and Cl have been recognized as impurities (as mentioned in the XRD pattern, Figures 1 and 2). Elemental mapping confirms the uniform distribution of CdSe particles within the PANI matrix. The mixing method effectively produced a stable physical composite, as supported by structural, microstructural, and chemical analyses. Significant NaCl presence is observed alongside PANI and CdSe, as confirmed by overlapping Na and Cl maps. XRD results (Figures 1 and 2) also indicated that this impurity necessitates thorough washing. In Figure 11, the electron backscattered image reveals that the bright irregular agglomerates are quantum dots, NaCl particles

exhibit a sheet-like morphology, and the gray background is related to the PANI matrix.

3.5. Optical properties

Most researchers have synthesized CdSe QDs using hydrothermal [20, 21] or thermal methods at 280 °C in the presence of trioctylphosphine oxide (TOPO) [17]. Most research in this area has focused on co-precipitation methods at temperatures ranging from 0 °C to ambient temperature [33], with less research on co-precipitation in the temperature range of 70-100 °C in the presence of reducing and surface-modifying agents. The most important parameter affecting the particle formation process through nucleation and growth is the reaction temperature. The product obtained at different temperatures has different particle sizes, and as a result, the peak position and emission intensity shift due to being in the quantum confinement regime below the Bohr radius. The emission spectrum of CdSe QDs samples is shown in Figure 12. As shown in the figure, with increasing temperature from 70 to 100 °C, the emission peak shifts towards lower energies or higher wavelengths along with particle growth. The highest emission intensity corresponds to the sample synthesized at 90 °C. In other words, the highest radiative electron transition occurs in this sample. This can also be due to the best covering of the CdS passive shell on the surface of QDs, which prevents non-radiative electron transitions and increases the quantum yield. Therefore, only the CdSe QDs synthesized at 90 °C formed composite with PANI.

To investigate the band gap, the $(\alpha h\nu)^{0.5}$ vs. hν curve was plotted, as shown in Figure 13. As calculated from the curve, the bandgap value decreases from 3.2 eV in the sample synthesized at 70°C to 2.8 eV in the sample synthesized at 100°C, which confirms the changes in the emission spectra. This means that increasing the size of the particles with increasing the synthesis temperature leads to a decrease in the band gap.

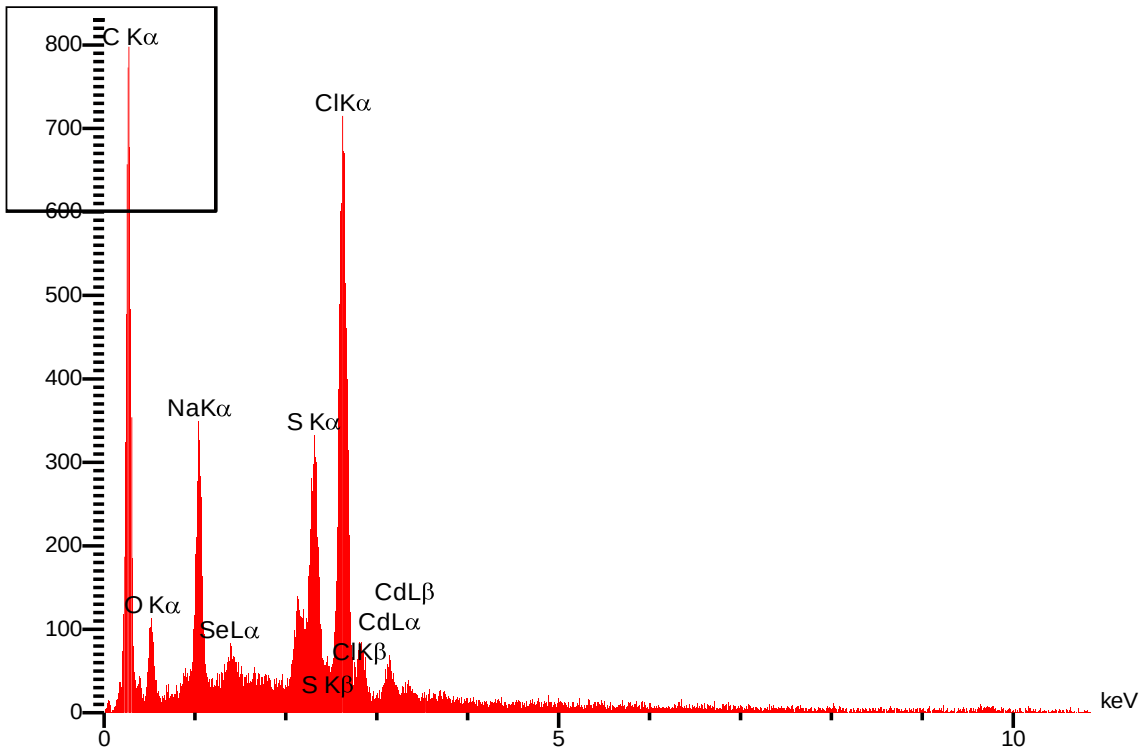

Figure 10: EDX analysis of CdSe QDs-PANI nanocomposite (In accordance with Figure 9c).

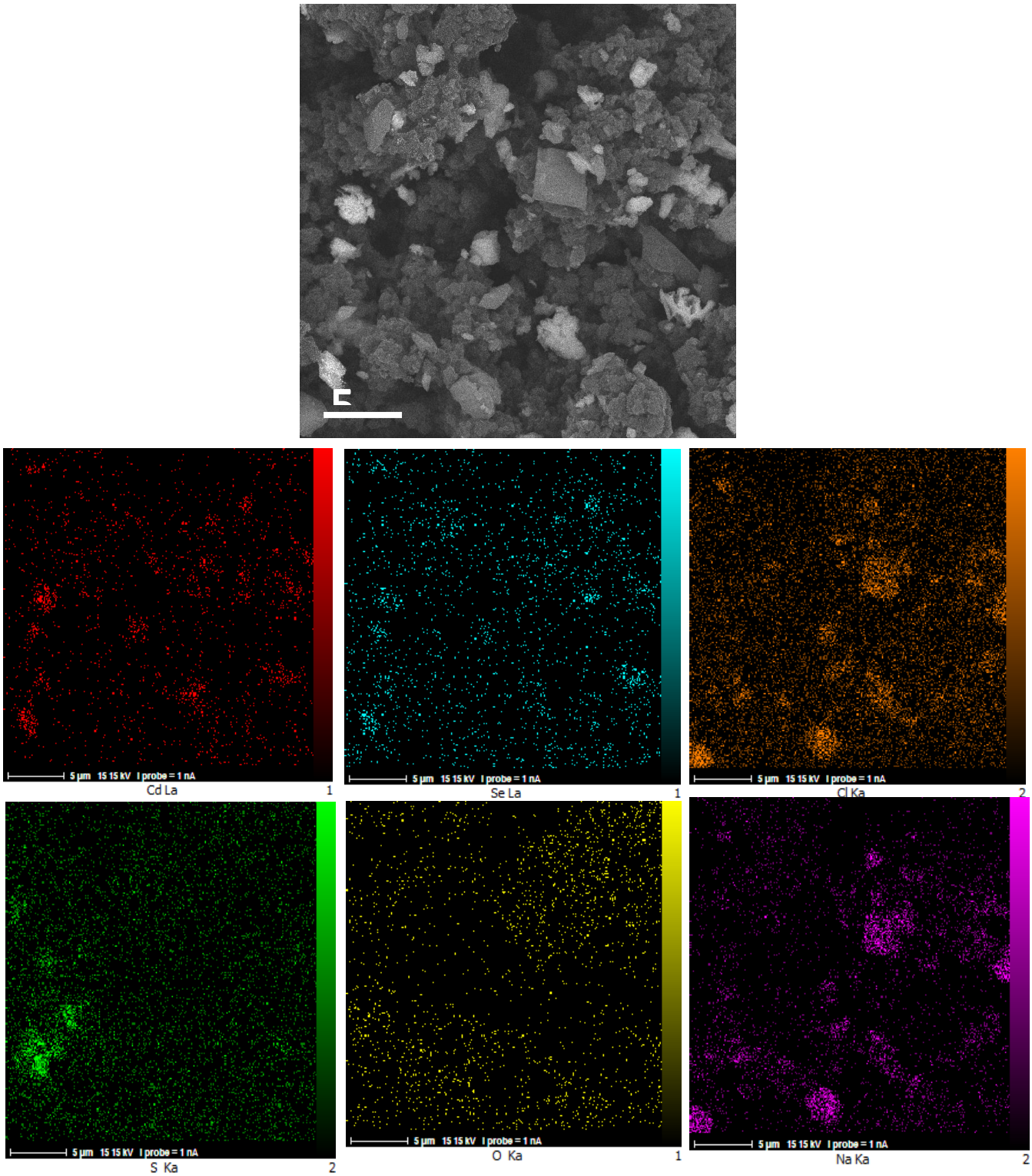

Figure 11: Elemental mapping of CdSe QDs-PANI nanocomposite.

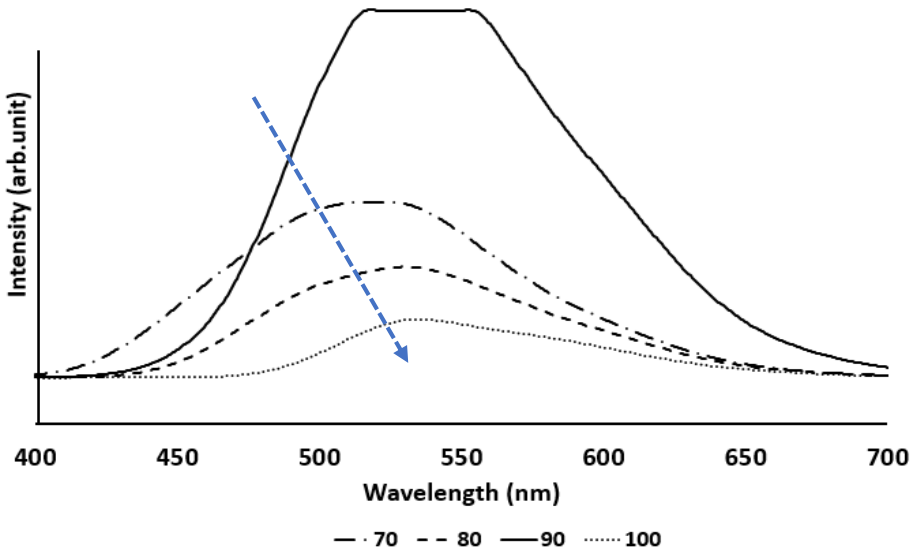

Figure 12: Photoluminescence spectra of the CdSe QDs synthesized at 70-100 °C.

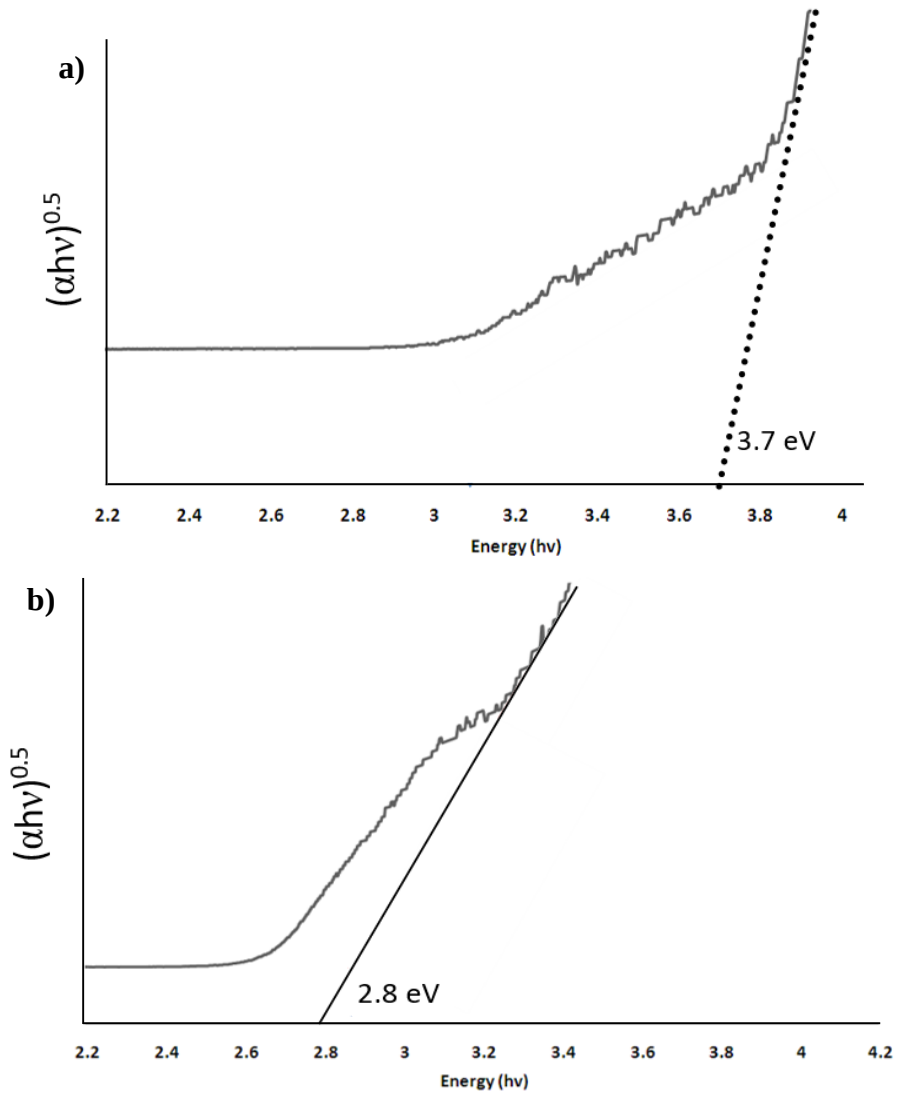

Figure 13: Band gap calculated by Tauc method for CdSe QDs synthesized at (a) 70°C, and (b) 100 °C.

Figure 14 shows the emission spectra of PANI and CdSe QDs-PANI nanocomposite. The emission spectra of the two samples with 5 and 10 weight percent QDs are referred to as PANI-low QDs and PANI-high QDs, respectively. The observed emission in all samples at around 428 nm is attributed to the π-π* benzenoid electronic transition in polyaniline [34]. Due to the polymeric structure and entanglement of particles, in the PANI-low QDs sample, the 360 nm excitation photons do not result in QD emission, whereas with increasing the concentration of quantum dots in the PANI-high QDs sample, an emission peak is observed in the green wavelength region around 550 nm.

Under irradiation, quantum dots are excited. With the movement of an electron to the valence band and leaving a hole in the conduction band, an exciton is formed. Due to the high surface area of these sub-5 nanometer particles, defects such as holes can be trapped within their interstitial spaces. The electron transition to these trapped surface levels forms the first emission mechanism, which has broad peaks. Along with the red shift of the excitation wavelength, the emission also shifts towards the red. If the surface is coated with capping agents and surfactants, exciton emission occurs, which is the second emission mechanism. By increasing the temperature or time, the emission shifts towards lower energies. This shift originates from the particle-in-a-box model or quantum confinement [35]; a larger box has a smaller band gap. Considering the broadness of the emission peaks, it appears that the synthesized CdSe QDs in different temperature ranges mainly follow the first emission mechanism. After the compositing process, the interaction between PANI and QDs leads to electron transfer from PANI to the surface levels of QDs due to the active surface traps. This electron transfer reduces the intrinsic emission of PANI and, as shown in Figure 14, increases the emission intensity of QDs.

The simultaneous presence of PANI and QDs led to improved thermal stability. In addition, the electro-optical interaction between these two composite components was also confirmed. The resulting composite is a suitable candidate for many applications such as optoelectronics, sensing, solar cells, and LEDs. The electrical conductivity behavior of PANI along with the luminescence properties of QDs is effective for fabricating efficient LEDs. In solar cells, QDs increase efficiency due to the production of electron-hole pairs. This composite can also contribute to better electrical, environmental and mechanical of biosensors.

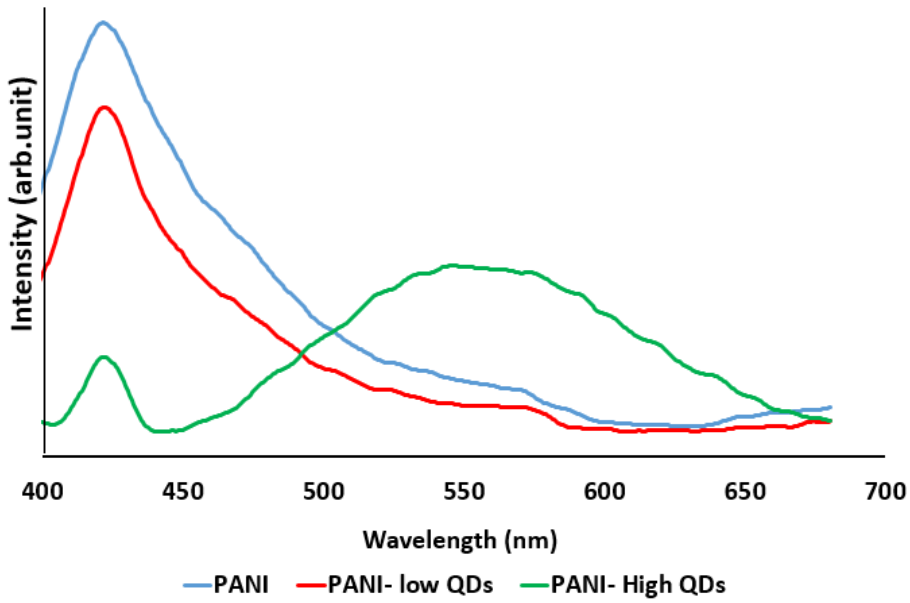

Figure 14: Photoluminescence spectra of the PANI, PANI- low QDs, and PANI- high QDs.

4. Conclusion

CdSe QDs-PANI nanocomposites were synthesized via polymerization process. XRD and FTIR results revealed the existence of PANI and CdSe QDs compounds and phases in the compositing process. The Composite showed 10 % by weight decrease of weight loss after heating to 600 °C by compared to the PANI due to the higher stability of QDs. Morphological studies demonstrated that the PANI particles formed agglo-merated nanorods in a honeycomb-like form, while CdSe QDs were detected as disordered hard masses. The nanocomposite was consisted of a matrix of PANI nanorods along with amorphous CdSe particles that were trapped regularly in the matrix cavities. EDX and elemental mapping results confirmed the presence of PANI, CdSe, and a small amount of sheet-like NaCl impurities. The emission of CdSe QDs showed that the peak wavelength and intensity of blue to green emission (with the highest intensity for the sample synthesized at 90 °C) being highly dependent on the synthesis temperature. In addition, the bandgap decreased from about 3.2 eV to 2.8 eV with an increase in temperature from 70 to 100 °C, because of quantum confinement effect. The emission spectrum of PANI showed a peak in the blue region (428 nm) related to the π-π* benzenoid electronic transition. Increasing the concentration of QDs to 10 % by weight relative to PANI resulted in the observation of the QDs emission peak at 550 nm and a decrease in the intensity of the blue peak of PANI due to a successful electronic interaction between the PANI and QDs.

5. References

1. Manna L. The bright and enlightening science of quantum dots. Nano Lett. 2023; 23(21): 9673-76. https://doi.org/10.1021/acs.nanolett.3c03904.
2. Cotta MA. Quantum dots and their applications: what lies ahead?. ACS Appl Nano Mater. 2018;3(6): 4920-24. https://doi.org/10.1021/acsanm.0c01386.
3. Bera D, Qian L, Tseng TK, Holloway PH. Quantum Dots and Their Multimodal Applications: A Review. Materials. 2010;3(4):2260-2345. https://doi.org/10. 3390/ma3042260.
4. Agarwal K, Rai H, Mondal S. Quantum dots: an overview of synthesis, properties, and applications. Mater Res Express. 2023; 10(6):062001. https://doi. org/10.1088/2053-1591/acda17.
5. Gidwani B, Sahu V, Shukla SS, Pandey R, Joshi V, Jain VK, et al. Quantum dots: Prospective, toxicity, advances and applications. J Drug Deliv Sci Tec. 2021;61:102308. https://doi.org/10.1016/j.jddst. 2020. 102308.
6. Asadi F, Jannesari A, Arabi AM. Synthesis and Characterization of Well-dispersed Zinc oxide quantum dots in epoxy resin using epoxy siloxane surface modifier. Prog Color, Colorants Coat. 2023; 16(4): 399-408. https://doi.org/10. 30509/pccc.2023. 167118.1210.
7. Kausar A. Polyaniline and quantum dot-based nanostructures: developments and perspectives. J Plast Film Sheet. 2020;36(4):430-447. https://doi.org/ 10. 1177/8756087920926649.
8. Kehlbeck JD, Hagerman ME, Cohen BD, Eliseo J, Fox M, Hoek W, et al. Directed self-assembly in laponite/CdSe/polyaniline nanocomposites. Langmuir. 2008;24(17):9727-38. https://doi.org/10.1021/la800 953w.
9. Patidar D, Jain N, Saxena NS, Sharma K, Sharma. Electrical Properties of CdS/Polyaniline Hetero-junction. Braz J Phys. 2006;36(4):1210-12. https://doi.org/10.1590/S0103-97332006000700016.
10. Yadav A, Kumar H, Sharma R, Kumari R, Thakur M. Quantum dot decorated polyaniline plastic as a multifunctional nanocomposite: experimental and theoretical approach. RSC Adv. 2022, 12(37), 24063-76.https://doi.org/10.1039/d2ra03554.
11. Mehare MD, Deshmukh AD, Dhoble SJ. Carbon quantum dots/polyaniline nanocomposite (S-CQD/ PANI) for high capacitive asymmetric supercapacitor device. J Nanosci Nanotechnol. 2020; 20(6):3785-94. https://doi.org/10.1166/jnn.2020. 17778.
12. Ganganboina AB, Doong RA. Graphene quantum dots decorated gold-polyaniline nanowire for impedimetric detection of carcinoembryonic antigen. Sci Rep. 2019;9:7214. https://doi.org/10.1038/s41598-019-43740-3.
13. Shokry A, Khalil MMA, Ibrahim H, Soliman M, Ebrahi S. Highly luminescent ternary nano-composite of polyaniline, silver nanoparticles and graphene oxide quantum dots. Sci Rep. 2019;9: 16984. https://doi.org/ 10.1038/s41598-019-53584-6.
14. Rabia M, Mohamed HSH, Shaban M, Taha S. Preparation of polyaniline/PbS core-shell nano/ microcomposite and its application for photo-catalytic H_2 electrogeneration from H_2O. Sci Rep. 2018; 8: 1107. https://doi.org/10.1038/s41598-018-19326-w.
15. Ahilfi DN, Alkabbi AS, Mohammed KA, Ziadan KM. Fabrication and characterization of polyaniline/ cdse device for applications in nano structured solar cells. IOP Conf Ser: Mater Sci Eng. 2020; 928(7): 072069. https://doi.org/10.1088/1757-899X/ 928/7/ 072069.

16. Xu D, Yang M, Liu Y, Zhu R, Lv X, Zhang C, et al. Fabrication of an innovative designed TiO_2 nanosheets/CdSe/polyaniline/graphene quaternary composite and its application as in-situ photocathodic protection coatings on 304SS. J Alloy Compd. 2020; 822: 153685. https://doi.org/10.1016/j.jallcom.2020.153685.
17. Xu L, Huang X, Dai W, Sun P, Chen X, An L. Charge and energy transfer between cdse quantum dots and polyaniline. J Nanosci Nanotechnol. 2016;16 (4):3909-13. https://doi.org/10.1166/jnn.2016. 11851.
18. Abdul-Manaf NA, Echendu OK, Fauzi F, Bowen L, Dharmadasa IM. Development of polyaniline using electrochemical technique for plugging pinholes in cadmium sulfide/cadmium telluride solar cells. J Electron Mater. 2014; 43(9):4003–10. https://doi.org/10.1007/s11664-014-3361-5.
19. Shieh YT, Lu YT, Wang TL, Yang CH, Lin RH. Electrocatalytic activities of Nafion/CdSe/Self-doped polyaniline composites to dopamine, uric acid, and ascorbic acid. J Solid State Electrochem. 2014; 18: 975–984. https://doi.org/10.1007/s10008-013-2344-4.
20. Karimi B, Shafiee Afarani M, Arabi AM. Hydrothermal synthesis of cadmium selenide quantum dots: effect of reducing agent. Appl Phys A. 2020; 126, 706. https://doi.org/10.1007/s00339-020-03903-w.
21. Mahmoodi NM, Oveisi M, Arabi AM, Karimi B. Cadmium selenide quantum dots: synthesis, characterization, and dye removal ability with UV irradiation. Desalin Water Treat. 2015; 57(35), 16552–58. https://doi.org/10.1080/19443994.2015.1079259.
22. Haldorai Y, Nguyen VH, Shim JJ. Synthesis of polyaniline/Q-CdSe composite via ultrasonically assisted dynamic inverse emulsion polymerization. Colloid Polym Sci. 2011;289:849–854. https://doi.org/10.1007/s00396-011-2400-5.
23. Mostafaei A, Zolriasatein A. Synthesis and characterization of conducting polyaniline nano-composites containing ZnO nanorods. Prog Nat Sci-Mater. 2012;22(4):273-280. https://doi.org/10.1016/j.pnsc.2012.07.002
24. Hamizi NA, Ying CS, Johan MR. Synthesis with different se concentrations and optical studies of cdse quantum dots via inverse micelle technique. Int J Electrochem Sc. 2012;7(5),4727-34. https://doi.org/10.1016/S1452-3981(23)19577-0.
25. Vo NT, Ngo HD, Vu DL, Duong AP, Lam QV. Conjugation of E. coli O157:H7 Antibody to CdSe/ZnS Quantum Dots. J Nanomater. 2015; 1, 265315. https://doi.org/10.1155/2015/265315.
26. Shao W, Jamal R, Xu F, Ubul A, Abdiryim T. The effect of a small amount of water on the structure and electrochemical properties of solid-state synthesized polyaniline. Mater. 2015;5(10);1811-1825. https://doi.org/10.3390/ma5101811.
27. Bhadra S, Khastgir D. Glass–rubber transition temperature of polyaniline: Experimental and molecular dynamic simulation. Synthetic Met, 2009;159(12): 1141-1146. https://doi.org/10.1016/j.synthmet.2009.01.052.
28. Alves WF, Malmonge JA, Mattoso LH, Medeiros ES. Non-isothermal decomposition kinetics of conductive polyaniline and its derivatives. Polímeros. 2018;28 (4):285-92. https://doi.org/10.1590/0104-1428. 03116.
29. Kumar A, Kumar A, Mudila H, Kumar V. Synthesis and thermal analysis of polyaniline (PANI). J. Phys.: Conf. Ser. 2020;1531(1):012108. https://doi.org/10.1088/1742-6596/1531/1/012108.
30. Chao D, Chen J, Lu X, Chen L, Zhang W, Wei Y. SEM study of the morphology of high molecular weight polyaniline. Synthetic met. 2005;150(1):47-51. https://doi.org/10.1016/j.synthmet.2005.01.010.
31. Sedaghat S, Golbaz F. In situ oxidative polymerization of aniline in the presence of manganese dioxide and preparation of polyaniline/MnO_2 nanocomposite. J Nanostruct Chem. 2013;3:65. https://doi.org/10.1186/2193-8865-3-65.
32. Freitas TV, Sousa EA, Fuzari Jr GC, Arlindo EP. Different morphologies of polyaniline nanostructures synthesized by interfacial polymerization. Mater Let. 2018; 224: 42-5. https://doi.org/10.1016/j.matlet.2018.04.062.
33. Sun Q, Fu S, Dong T, Liu S, Huang C. Aqueous synthesis and characterization of TGA-capped CdSe quantum dots at freezing temperature. Molecules. 2012; 17(7):8430-8. https://doi.org/10.3390/molecules17078430.
34. Ahmed SU, Akter F, Oliullah MD, Chowdhury MSH, Talukder MDM, Pramanik SK, et al. Role of reaction time on the electrical conductivity, thermal stability and photoluminescence property of polyanilne nanofibers. Int J Chem React Eng. 2020; 18(1): 20190088. https://doi.org/10.1515/ijcre-2019-0088.
35. Landry ML, Morrell TE, Karagounis TK, Hsia CH, Wang CY. Simple syntheses of CdSe quantum dots. J Chem Educ. 2014; 91(2), 274–279. https://doi.org/10.1021/ed300568e.

How to cite this article:
Arabi AM, Shirkavand Hadavand B. Polyaniline-CdSe quantum dot nanostructure: characterization and properties. Prog Color Colorants Coat. 2025;18(4):445-459. https://doi.org/10.30509/pccc.2025.167441.1348.